Dynamical Fano-Like Interference between Rabi Oscillations and Coherent Phonons in a Semiconductor Microcavity System

S. Yoshino, G. Oohata, and K. Mizoguchi
Department of Physical Science, Graduate School of Science, Osaka Prefecture University, 1-1 Gakuen-cho, Naka-ku, Sakai 599-8531, Japan
(Received 19 March 2015; published 7 October 2015)

We report on dynamical interference between short-lived Rabi oscillations and long-lived coherent phonons in CuCl semiconductor microcavities resulting from the coupling between the two oscillations. The Fourier-transformed spectra of the time-domain signals obtained from semiconductor microcavities by using a pump-probe technique show that the intensity of the coherent longitudinal optical phonon of CuCl is enhanced by increasing that of the Rabi oscillation, which indicates that the coherent phonon is driven by the Rabi oscillation through the Fröhlich interaction. Moreover, as the Rabi oscillation frequency decreases upon crossing the phonon frequency, the spectral profile of the coherent phonon changes from a peak to a dip with an asymmetric structure. The continuous wavelet transformation reveals that these peak and dip structures originate from constructive and destructive interference between Rabi oscillations and coherent phonons, respectively. We demonstrate that the asymmetric spectral structures in relation to the frequency detuning are well reproduced by using a classical coupled oscillator model on the basis of dynamical Fano-like interference.

DOI: 10.1103/PhysRevLett.115.157402 PACS numbers: 78.47.J-, 71.36.+c, 78.67.Pt, 82.53.Mj

Dynamical coupling between two states provides a rich variety of ultrafast phenomena [1,2]. Fano interference resulting from the interaction between discrete and continuum states shows asymmetric spectral profiles as the spectroscopic signatures of atoms, semiconductors, and nanomaterials [3,4]. The dynamical behavior of the Fano interference in various materials has been reported [5–10]. On the other hand, it is well known that an anticrossing appears in the spectrum when two resonance states with sufficiently slow relaxation rates as compared with a coupling rate are strongly coupled. When quantum beats [11] and Bloch oscillations [12] are coupled to coherent longitudinal optical (LO) phonons, these phonons are significantly enhanced and coupled modes appear [13–16]. Here, quantum beats and Bloch oscillations originate from quantum interference between two excited states under simultaneous excitation by ultrashort laser pulses. Moreover, phonons impulsively generated by ultrashort laser pulses are referred to as coherent phonons, which have coherence in time and space [17,18].

In contrast to the coupling phenomenon between two discrete states with slow relaxation rates, we consider that it is an intriguing subject to investigate the dynamical coupling between the fast-relaxing and slow-relaxing discrete states. Since Rabi oscillations (ROs) with fast relaxation rates in semiconductor microcavities [19–21] are also quantum oscillations resulting from quantum interference between two polariton states, the exciton components of these polaritons are expected to couple to coherent LO phonons (CPs) with slow relaxation rates through the Fröhlich interaction.

We can represent the coupling between the fast-relaxing RO and the slow-relaxing CP in the semiclassical picture by two coupled transient states in which the energy widths are related to the relaxation rates (Fig. 1). The excited state in this picture is the fast-relaxing oscillation that has a broad energy band, which is similar to a continuum state. When this state couples to the excited state with a sharp energy band, we speculate that the Fourier-transformed (FT) spectra of the time-domain signals will have an asymmetric profile, similar to the frequency-domain spectrum of the common Fano interference.

In this Letter, we report the first observation of the dynamical coupling and interference between fast-relaxing ROs and slow-relaxing CPs in CuCl semiconductor microcavities. The oscillatory signals obtained in the

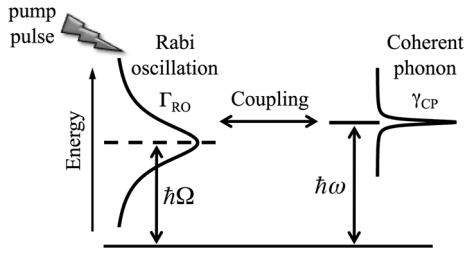

FIG. 1. Schematic diagram of coupled oscillator model connecting a fast-relaxing RO (broad spectrum) and a slow-relaxing CP (sharp spectrum). $\hbar\Omega$ and $\hbar\omega$ indicate the RO and CP energies, respectively; Γ_{RO} and γ_{CP} are the RO and CP relaxation rates, respectively ($\Gamma_{RO} > \gamma_{CP}$). When the RO and CP are resonant in energy, they couple through the Fröhlich interaction between the LO phonons and the excitonic components of the RO.

microcavities by using a pump-probe technique demonstrate that the amplitude of the CP oscillation is enhanced by increasing that of the RO, which indicates the generation of a RO-driven CP. Moreover, it is found that the spectral profile of the CP mode drastically changes with the RO frequency, which implies dynamical Fano-like interference. We discuss the spectral change of the CP mode by comparing it with a classical coupled oscillator model [22].

The spectral profiles for Fano interference are discussed using classical equations of motion for coordinates associated with the discrete and continuum states, which is called a classical Fano oscillator model [22]. The interference between the broad and sharp excited states of two oscillations in this study is treated as classical equations for coupled oscillations by extending a classical Fano oscillator model. When the polarization Q associated with the excitonic component of a RO couples linearly to the polarization q of a CP through the Fröhlich interaction with coupling constant C, the equations for coupled oscillations are given by [22]

$$\frac{d^2Q}{dt^2} + 2\Gamma_{\mathrm{RO}}\frac{dQ}{dt} + \Omega^2 Q + Cq = F_Q,$$
$$\frac{d^2q}{dt^2} + 2\gamma_{\mathrm{CP}}\frac{dq}{dt} + \omega^2 q + CQ = F_q. \quad (1)$$

Here, Ω and ω are the undamped angular frequencies of the RO and CP, respectively, Γ_{RO} and γ_{CP} are the relaxation rates of the RO and CP, and F_Q and F_q are the driving forces for the generation of the RO and CP. The relaxation rate of the RO, which is faster than that of the CP, corresponds to the inverse of the coherence time between two polariton states. The damped angular frequencies are given by $\Omega_{\mathrm{RO}} = \sqrt{\Omega^2 - \Gamma_{\mathrm{RO}}^2}$ and $\omega_{\mathrm{CP}} = \sqrt{\omega^2 - \gamma_{\mathrm{CP}}^2}$. We assume that the coupling constant is very small ($C \ll \omega\Omega$), and that the pump pulse excites only a RO, and successively the RO generates a CP: $F_Q \propto \delta(t)$ and $F_q = 0$, where $\delta(t)$ is the Dirac delta function. The total oscillatory polarization $f(t)$ generated by the coupling between the RO and CP is represented by [23]

$$f(t) = f_{\mathrm{RO}}(t) + f_{\mathrm{RO+CP}}(t), \quad (2)$$

where f_{RO} and $f_{\mathrm{RO+CP}}$ indicate the forced oscillatory polarization of the RO driven by F_Q and the weakly coupled oscillatory polarization between the RO and CP, respectively. $f_{\mathrm{RO+CP}}$ comprises the oscillatory polarizations of the RO and CP with a phase shift. Hereafter, we refer to $f_{\mathrm{RO+CP}}$ as the "coupled CP." The time evolution of $f(t)$ exhibits the transient interference between the RO and the coupled CP. This transient interference will cause changes in the FT spectrum of $f(t)$.

The schematic structure of the CuCl microcavity fabricated is shown in Fig. 2(a) [31,32]. In a fabricated CuCl microcavity on a (0001) Al_2O_3 substrate, a cavity layer is sandwiched between a top distributed Bragg reflector (DBR) with 4 periods and a bottom DBR with 4.5 periods. The layers constituting DBRs consist of dielectric materials $PbCl_2$ and AlF_3 with layer thicknesses of $\lambda/4$. The cavity layer (thickness $L_{\mathrm{cav}} = \lambda$) consists of a CuCl active layer (thickness $L_{\mathrm{act}} = \lambda/8$) sandwiched by AlF_3 spacer layers. Here, $\lambda = \lambda_{\mathrm{ex}}/n_b$, where λ_{ex} is the resonant wavelength of the Z_3 exciton of CuCl in vacuum ($\lambda_{\mathrm{ex}} = 387$ nm) and n_b is the background refractive index [33]. The quality factor of the fabricated microcavity is approximately 160, which results in relaxation rates for the ROs that are faster than 4 ps^{-1}. The Rabi splitting energy of the CuCl microcavity can be made approximately equal to the CP frequency by varying the active layer thickness. The angle-resolved transmission spectra were obtained at 10 K using a 32-cm single monochromator combined with a charge-coupled device camera [23].

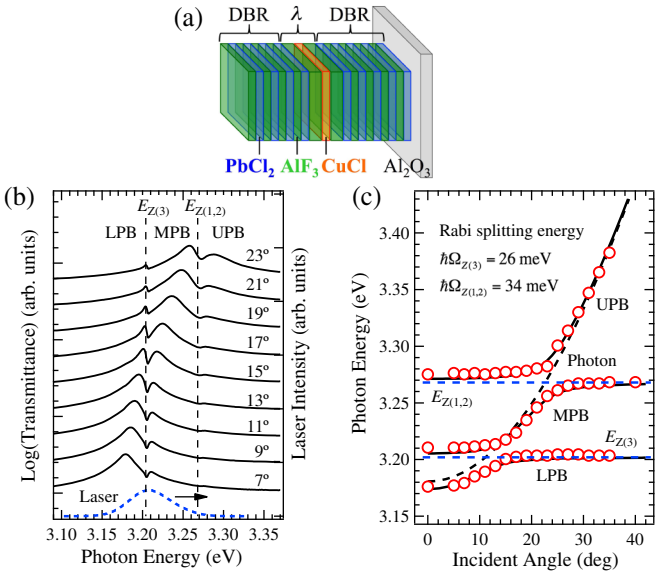

FIG. 2 (color online). (a) Schematic of the CuCl microcavity structure with DBRs. (b) Transmission spectra of the CuCl microcavity for various incident angles at 10 K. The dashed vertical lines denote the energies of the Z_3 and $Z_{1,2}$ excitons: $E_{Z(3)}(E_{Z(1,2)}) = 3.202\,(3.268)$ eV. The blue dotted line represents the laser pulse spectrum for which the center energy was tuned to the energy midway between the LPB and MPB. (c) Incident angle dependence of peak energies of cavity polariton modes in the CuCl microcavity (open circles) and calculated dispersion relationship of the cavity polaritons (solid curves). The dashed curve gives the dispersion relationship of the cavity photon. The estimated Rabi splitting energies for the Z_3 and $Z_{1,2}$ excitons are 26 and 34 meV, respectively.

The transmittance spectra of the CuCl microcavity observed at various incident angles of white light are shown in Fig. 2(b). Three peaks varying with the incident angle originate from the coupling between the cavity photon and the Z_3 ($Z_{1,2}$) exciton [31,32]. These peaks indicate the cavity polariton modes, which are the lower

polariton branch (LPB), the middle polariton branch (MPB), and the upper polariton branch (UPB), in order of increasing energy. The peak energies of the cavity polariton modes are plotted as a function of incident angle in Fig. 2(c). The three solid curves represent the dispersion relationship of the cavity polariton fitted to the experimental results using a phenomenological 3×3 Hamiltonian. In the fabricated microcavity, the energy difference between the MPB and LPB can be controlled over a range that includes the LO phonon energy of CuCl ($\hbar\omega_{CP} = 26$ meV, $\omega_{CP}/2\pi = 6.3$ THz) [33] by varying the incident angle of pump pulses in a pump-probe technique, while that between the MPB and UPB does not decrease across the LO phonon energy. Then, we focus on the ROs between the MPB and LPB in the CuCl microcavity.

The oscillatory polarization due to the RO and CP generated by pump pulses modulates the complex dielectric function, which causes a temporal change in the transmissivity or reflectivity. In this study, we adopted an experimental method for observing the anisotropic change in the transmissivity, which is sensitive to the longitudinal oscillatory polarization [18]. Time-domain signals of the CuCl microcavities were measured at 10 K by a transmission-type electro-optic sampling method [18] with second-harmonic pulses of the mode-locked Ti:sapphire pulse laser delivering about 60-fs pulses [23]. The center of the laser pulses was tuned to about 3.209 eV, which was the central energy between the LPB and MPB, as shown in Fig. 2(b). The power densities of the pump and probe pulses were kept at approximately 0.1 and 0.01 μJ/cm^2, respectively.

The transient oscillatory signals from the CuCl microcavity obtained at various incident pump angles are shown in Fig. 3(a). Two oscillatory components are observed: a strong oscillation with a short relaxation time and a weak oscillation with a long relaxation time. To identify these strong and weak oscillations, we divided the oscillatory signals into two time regions (before and after 1.0 ps) and performed the time-partitioned Fourier transformation. The time-partitioned FT spectra of the two oscillatory signals observed at 15° pump incidence are shown in Fig. 3(b). For the time-partitioned FT spectrum of the oscillatory signal before 1.0 ps, the broad band results primarily from the RO between the MPB and LPB. The sharp peak at approximately 6.3 THz observed after 1.0 ps is attributed to the CP component after the RO relaxation. To clarify the coupling between the two oscillations, we investigated the relationship between the intensities of the RO and CP components for various incident pump angles, as plotted in Fig. 3(c). The square of the product of the transmission intensities at the LPB and MPB, $(T_{LPB}T_{MPB})^2$, which is evaluated by multiplying the transmittance spectra by the spectral profile of laser pulses in Fig. 2(b), is also shown. The incident angle dependence of the RO intensity is almost consistent with that of $(T_{LPB}T_{MPB})^2$ [34,35]. This

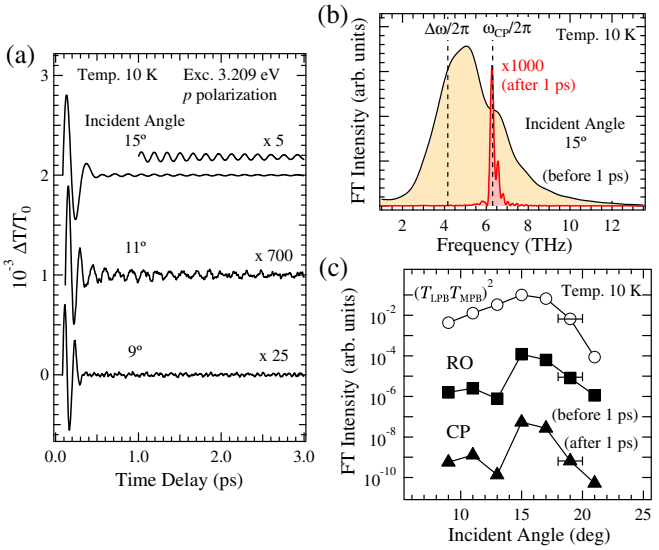

FIG. 3 (color online). (a) Oscillatory signals in the CuCl microcavity at various incident pump angles obtained at 10 K. (b) Time-partitioned FT spectra of oscillatory signals observed at incident pump angle of 15°. The black and red curves indicate the time-partitioned FT spectra of the oscillatory signals before and after 1 ps, respectively. The dotted vertical lines indicate the LO phonon frequency of CuCl ($\omega_{CP}/2\pi$) and the frequency ($\Delta\omega/2\pi$) corresponding to the energy difference between the MPB and LPB. (c) Incident angle dependence of intensities of the RO (squares) and CP (triangles) components in the time-partitioned FT spectra before and after 1 ps, respectively. The open circles show the square of the product of the transmission intensities at the LPB and MPB [$(T_{LPB}T_{MPB})^2$].

result indicates that the RO originates from the quantum interference between the LPB and MPB. Furthermore, the RO and CP intensities have a similar dependence on incident pump angle, which demonstrates that the CP oscillation is driven by the RO. When the RO frequency is close to the CP frequency, $\Omega_{RO} \sim \omega_{CP}$, it is expected that the CP intensity will be enhanced [13–16]. However, the actual enhancement factor occurring around 11° is very small. This small enhancement factor results from the rapid dephasing of the RO due to the small quality factor and the weak coupling between the RO and CP. The coupling constant is explained by taking account of the spatial structures of polarizations due to the excitons and CPs confined in the CuCl active layer. Moreover, a dip appears at an incident angle above the small peak at 11°. Although this asymmetric dip and peak structure might suggest Fano interference between the RO and CP, further investigations are required to confirm the origin of the dip.

The time-partitioned FT spectra shown in Fig. 3(b) indicate that the RO band is dominantly observed before 1.0 ps and the CP component survives well after the RO relaxation. As mentioned above, we speculate that the transient interference between the fast-relaxing RO and coupled CP will modify the FT spectra. To reveal this

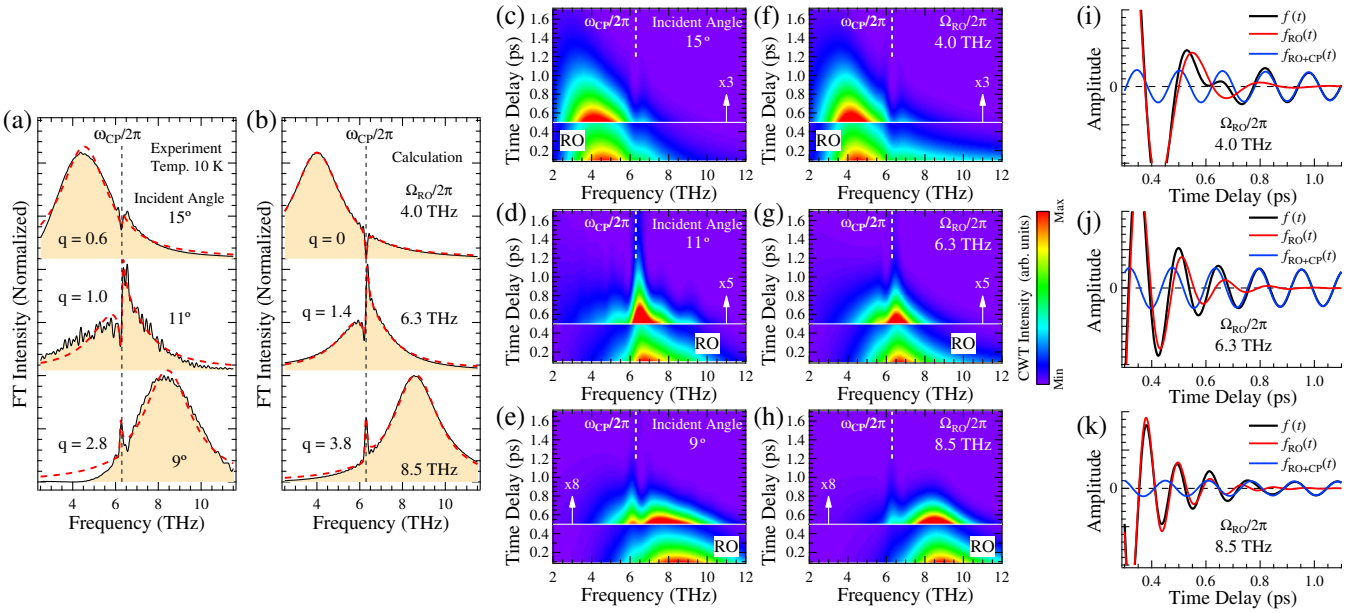

FIG. 4 (color online). (a) FT spectra of oscillatory signals for incident pump angles of 15°, 11°, and 9° observed at 10 K. (b) FT spectra of $f(t)$ calculated at $\Omega_{\mathrm{RO}}/2\pi = 4.0$, 6.3, and 8.5 THz. The Fano parameter q estimated by fitting the superposition of a Fano line shape and a Lorentz function to each FT spectrum is shown as a reference, where the red broken line indicates the fitted curve. (c)–(e) Image plots of CWT of oscillatory signals observed at 15°, 11°, and 9°, respectively. (f)–(h) Image plots of CWT of $f(t)$ calculated at $\Omega_{\mathrm{RO}}/2\pi = 4.0$, 6.3, and 8.5 THz, respectively. The vertical dashed line indicates the LO phonon frequency of CuCl, $\omega_{\mathrm{CP}}/2\pi$. (i)–(k) Temporal variations of f_{RO} (red line), $f_{\mathrm{RO+CP}}$ (blue line), and $f(t)$ (black line) at $\Omega_{\mathrm{RO}}/2\pi = 4.0$, 6.3, and 8.5 THz.

modification due to the transient interference, we performed a Fourier transformation of the oscillatory signals over the entire time range [Fig. 4(a)]. For increasing incident pump angle, the frequency of the RO band decreases upon crossing the CP frequency, which drastically changes the entire spectral profile. The coupled CP mode peaks over the broad RO band for $\Omega_{\mathrm{RO}} > \omega_{\mathrm{CP}}$ and dips for $\Omega_{\mathrm{RO}} < \omega_{\mathrm{CP}}$. In particular, for $\Omega_{\mathrm{RO}} \sim \omega_{\mathrm{CP}}$, the coupled CP mode has an asymmetric structure over the broad RO band. To reproduce the spectral profile of the coupled CP mode over the RO band, the FT spectra of $f(t)$ in Eq. (2) are calculated for various detuning frequencies between the RO and CP corresponding to the incident pump angle [Fig. 4(b)]. In this calculation, the values of Γ_{RO} and γ_{CP} can be estimated from the experimentally obtained FT spectra: $\Gamma_{\mathrm{RO}} = 8.5\,\mathrm{ps}^{-1}$ and $\gamma_{\mathrm{CP}} = 0.25\,\mathrm{ps}^{-1}$. The coupling constant is estimated by comparing the calculated FT spectra with the experimentally obtained FT spectra, which yields $\sqrt{C}/2\pi = 0.4$ THz. The calculated FT spectra agree well with the experimental results. This agreement demonstrates that dynamical Fano-like interference occurs between the two discrete states with fast and slow relaxation rates. Moreover, it is clear that the spectral structure can be controlled by varying the detuning frequency between the RO and CP.

Next, we performed the continuous wavelet transformation (CWT) of the oscillatory signals to reveal the dynamical interference between the RO and the coupled CP [36]. Figures 4(c)–4(h) show the image plots of CWT of the observed oscillatory signals and $f(t)$ calculated by Eq. (2). At 15°, corresponding to $\Omega_{\mathrm{RO}} < \omega_{\mathrm{CP}}$, a dip at $\omega_{\mathrm{CP}}/2\pi$ appears around 0.7 ps, which indicates that the coupled CP mode is suppressed by transient destructive interference from the RO [7]. In contrast, the coupled CP mode is observed for 9°, corresponding to $\Omega_{\mathrm{RO}} > \omega_{\mathrm{CP}}$, which indicates constructive interference. Moreover, at 11°, corresponding to $\Omega_{\mathrm{RO}} \sim \omega_{\mathrm{CP}}$, a peak and a dip around $\omega_{\mathrm{CP}}/2\pi$ are observed, which reflects the asymmetric structure of the coupled CP. To clarify the origin of destructive and constructive interference, the time evolution of f_{RO} and $f_{\mathrm{RO+CP}}$ is compared in Figs. 4(i) and 4(k). When the amplitudes of f_{RO} and $f_{\mathrm{RO+CP}}$ are nearly the same, f_{RO} oscillates in phase with $f_{\mathrm{RO+CP}}$ for $\Omega_{\mathrm{RO}} > \omega_{\mathrm{CP}}$, but oscillates out of phase when $\Omega_{\mathrm{RO}} < \omega_{\mathrm{CP}}$. This indicates that the phase difference between f_{RO} and $f_{\mathrm{RO+CP}}$ causes the peak and dip structures in the spectrum of the coupled CP mode. In particular, for $\Omega_{\mathrm{RO}} \sim \omega_{\mathrm{CP}}$, the phase difference between f_{RO} and $f_{\mathrm{RO+CP}}$ shown in Fig. 4(j) is approximately $\pi/2$; therefore, the asymmetric structure of the coupled CP mode appears clearly, as shown in Fig. 4(a). Thus, the asymmetry of the coupled CP mode originates from the phase difference between the RO and the coupled CP.

In summary, we have investigated the dynamical coupling and interference between a RO and a CP in a CuCl semiconductor microcavity. The time-domain signals

observed in the microcavities demonstrate that the CP is driven by the RO through the dynamical coupling between the two oscillations. Furthermore, when the RO frequency is decreased below the CP frequency, the spectral profile of the coupled CP mode drastically changes from a peak to a dip with an asymmetric structure. The asymmetric structure originates from the dynamical Fano-like interference between the short-lived RO and the long-lived coupled CP with a phase shift. This dynamical Fano-like interference is expected to play an important role in the dynamical coupling between two states, such as a steady state and a transient state in quantum devices.

This study was supported by the Japan Society for the Promotion of Science, KAKENHI Grants No. 23340087 and No. 24654090. We thank Professor H. Ishihara for useful discussions of the theory and Dr. S. S. Garmon for useful comments.

[1] J. Shah, in *Ultrafast Spectroscopy of Semiconductors and Semiconductor Nanostructures*, edited by M. Cardona, Springer Series in Solid-State Sciences (Springer, Berlin, 1996).
[2] F. Rossi and T. Kuhn, Rev. Mod. Phys. **74**, 895 (2002).
[3] U. Fano, Phys. Rev. **124**, 1866 (1961).
[4] A. E. Miroshnichenko, S. Flach, and Y. S. Kivshar, Rev. Mod. Phys. **82**, 2257 (2010).
[5] U. Siegner, M. A. Mycek, S. Glutsch, and D. S. Chemla, Phys. Rev. Lett. **74**, 470 (1995).
[6] C. P. Holfeld, F. Löser, M. Sudzius, K. Leo, D. M. Whittaker, and K. Köhler, Phys. Rev. Lett. **81**, 874 (1998).
[7] M. Hase, M. Kitajima, A. M. Constantinescu, and H. Petek, Nature (London) **426**, 51 (2003).
[8] M. Wickenhauser, J. Burgdörfer, F. Krausz, and M. Drescher, Phys. Rev. Lett. **94**, 023002 (2005).
[9] H. Wang, M. Chini, S. Chen, C.-H. Zhang, Y. Cheng, F. He, Y. Wu, U. Thumm, and Z. Chang, Phys. Rev. Lett. **105**, 143002 (2010).
[10] C. Ott, A. Kaldun, P. Raith, K. Meyer, M. Laux, J. Evers, C. H. Keitel, C. H. Greene, and T. Pfeifer, Science **340**, 716 (2013).
[11] E. O. Göbel, K. Leo, T. C. Damen, J. Shah, S. Schmitt-Rink, W. Schäfer, J. F. Müller, and K. Köhler, Phys. Rev. Lett. **64**, 1801 (1990).
[12] K. Leo, P. H. Bolivar, F. Brüggemann, R. Schwedler, and K. Köhler, Solid State Commun. **84**, 943 (1992).
[13] T. Dekorsy, A. Bartels, H. Kurz, K. Köhler, R. Hey, and K. Ploog, Phys. Rev. Lett. **85**, 1080 (2000).
[14] A. W. Ghosh, L. Jönsson, and J. W. Wilkins, Phys. Rev. Lett. **85**, 1084 (2000).
[15] O. Kojima, K. Mizoguchi, and M. Nakayama, Phys. Rev. B **68**, 155325 (2003).
[16] K. Mizoguchi, O. Kojima, T. Furuichi, M. Nakayama, K. Akahane, N. Yamamoto, and N. Ohtani, Phys. Rev. B **69**, 233302 (2004).
[17] R. Merlin, Solid State Commun. **102**, 207 (1997).
[18] T. Dekorsy, G. C. Cho, and H. Kurz, in *Light Scattering in Solids VIII*, edited by M. Cardona and G. Güntherodt (Springer-Verlag, Berlin, 2000).
[19] C. Weisbuch, M. Nishioka, A. Ishikawa, and Y. Arakawa, Phys. Rev. Lett. **69**, 3314 (1992).
[20] T. B. Norris, J.-K. Rhee, C.-Y. Sung, Y. Arakawa, M. Nishioka, and C. Weisbuch, Phys. Rev. B **50**, 14663 (1994).
[21] G. Khitrova, H. M. Gibbs, F. Jahnke, M. Kira, and S. W. Koch, Rev. Mod. Phys. **71**, 1591 (1999).
[22] D. M. Riffe, Phys. Rev. B **84**, 064308 (2011).
[23] See Supplemental Material at http://link.aps.org/supplemental/10.1103/PhysRevLett.115.157402, which includes Refs. [24–30], for sample structures, experimental methods, a continuous wavelet transformation, and a classical coupled oscillator model.
[24] J.-C. Diels and W. Rudolph, in *Ultrashort Laser Pulse Phenomena: Fundamentals, Techniques, and Applications on a Femtosecond Time Scale*, edited by P. F. Liao, P. L. Kelley, and I. Kaminow (Academic Press, San Diego, 1996).
[25] P. G. Savvidis, J. J. Baumberg, R. M. Stevenson, M. S. Skolnick, D. M. Whittaker, and J. S. Roberts, Phys. Rev. Lett. **84**, 1547 (2000).
[26] P. Tsotsis, P. S. Eldridge, T. Gao, S. I. Tsintzos, Z. Hatzopoulos, and P. G. Savvidis, New J. Phys. **14**, 023060 (2012).
[27] M. Saba, C. Ciuti, J. Bloch, V. Thierry-Mieg, R. Andre, Le Si Dang, S. Kundermann, A. Mura, G. Bongiovanni, J. L. Staehli, and B. Deveaud, Nature (London) **414**, 731 (2001).
[28] T. Tang, Y. Zhang, C. Park, B. Geng, C. Girit, Z. Hao, M. C. Martin, A. Zettl, M. F. Crommie, S. G. Louie, Y. R. Shen, and F. Wang, Nat. Nanotechnol. **5**, 32 (2010).
[29] V. Giannini, Y. Francescato, H. Amrania, C. C. Phillips, and A. Maier, Nano Lett. **11**, 2835 (2011).
[30] L. D. Landau and E. M. Lifshitz, *Mechanics*, 3rd ed. (Pergamon, New York, 1976).
[31] G. Oohata, T. Nishioka, D. Kim, H. Ishihara, and M. Nakayama, Phys. Rev. B **78**, 233304 (2008).
[32] S. Yoshino, G. Oohata, Y. Shim, H. Ishihara, and K. Mizoguchi, Phys. Rev. B **88**, 205311 (2013).
[33] O. Madelung, *Semicoductors: Data Handbook*, 3rd ed. (Springer-Verlag, Berlin, 2004).
[34] K. Leo, J. Shah, E. O. Göbel, T. C. Damen, S. Schmitt-Rink, W. Schäfer, and K. Köhler, Phys. Rev. Lett. **66**, 201 (1991).
[35] T. Hasegawa, K. Mizoguchi, and M. Nakayama, Phys. Rev. B **76**, 115323 (2007).
[36] C. K. Chui, *An Introduction to Wavelets* (Academic Press, San Diego, 1992).